Supplementary Information for

Spontaneous formation and growth kinetics of lipid nanotubules induced by passive nanoparticles

Roobala Chelladurai, Koushik Debnath, Nikhil R Jana and Jaydeep K Basu (complete author list)

Jaydeep K Basu.
E-mail: basu@iisc.ac.in

This PDF file includes:

Supplementary text
Figs. S1 to S21 (not allowed for Brief Reports)
SI References

Supporting Information Text

1. SI Appendix

A. (i) Sample Preparation. DLPC (1,2-Dilauroyl-sn-glycero-3-phosphocholine) and DPPC (1,2-dipalmitoyl-sn-glycero-3-phosphocholine) lipids were procured from Avanti lipids and ATTO 488 DMPE ((ATTO - Tec GmbH)), head tagged lipid and BODIPY C12 HPC (Life Technologies), tail tagged lipid fluoroscent dyes were used for tagging. Supported lipid bilayers used in the study has been prepared using Langmuir Blodgett (LB) technique and always stored under water to prevent dewetting. Samples were prepared suitable for confocal imaging by choosing a mixture of dye:lipid ratio of 1:10 000/1:100 000. SLBs were transferred at a surface pressure of 32 mN/m from a sub-phase of water maintained at temperature of T = 15 °C with up stroke dipper speed of 5 mm/min and down stroke speed of 3 mm/min. Transferred bilayers has been used for measurements immediate to transfer or within a few hours.

B. (ii) Characterization of Quantum Dots. Cadmium Selenide Zinc Sulfide (CdSe/ZnS) red emissive quantum dots (QDs) of hydrodynamic radius of 10 nm was synthesized using method reported in an earlier work. In brief, Se solution was injected into Cadmium Stearate solution in 1-octadecene at 280 °C to prepare CdSe nanoparticles. Further, zinc stearate solution and Se solution was injected consecutively at 290 C. Finally, hydrophilic QDs were prepared through polyacrylate coating. Characterization of the QD sample has been shown in Figure S1. Custom made polymer capped CdSe-ZnS QDs are red emissive with emission peak at $\sim$ 600 nm and hydrodynamic size of at $\sim$ 10 nm. QD incubation on bilayers was carried out in a liquid cell customized for confocal measurements that enables live capturing of structural and dynamical changes on the membrane on binding of QD. From a stock of 4 nM solution of the QD, 5 ul was added to the 1 ml of buffer present in the volume of the liquid cell containing the bilayer. The solution was mildly pipette aspirated in order to attain homogeneous mixing of the sample.

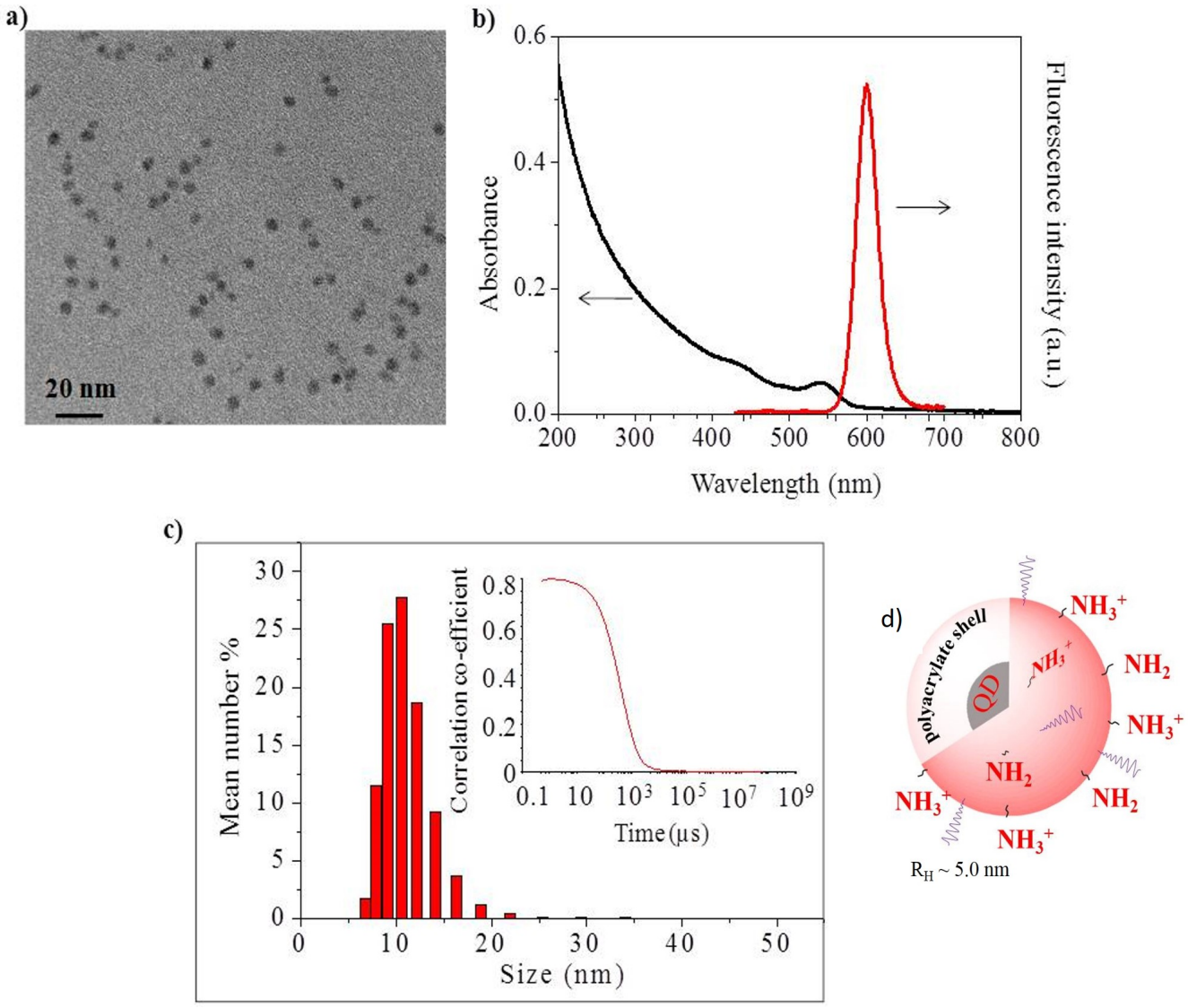

Fig. S1. QD characterization.
a) TEM images of CdSe-ZnS QDs b) Emission spectra showing a peak at $\sim$ 600 nm c) Hydrodynamic radius of $\sim$ 5 nm d) Schematics of the Amine terminated CdSe-ZnS QD with polyacrylate coating

C. (iii) Confocal Imaging. LEICA TCS SP5 II model was used in studying the structural evolution of the fluorescent tagged bilayers. Argon laser (488 nm) was used to excite both the green emissive lipid tag and the red emissive QD. All measurements were carried out using 63 x water immersion objective. Most of the data discussed in the main text is based on confocal microsopy based time dependent fluorescence imaging. Time series analysis has been carried out by capturing images successively or using xyt mode of image capture. Supported lipid bilayers (SLBs) were fixed on a glass coverslip using a double sided tap and mounted on the microscopy. Liquid cell used for this imaging was custom made and ensures that the SLBs are always maintained under water.

D. (iv) Unsupported Membrane platform (GUV). Most of the experimental studies on tubulation from artificial membranes employ GUVs as the choice of platform (1, 2). In order to set the comparison and to study the effect of QD binding in absence of any support, GUVs were also employed as one of the control experiments. Binding of QDs on DLPC GUVs resulted in budding of smaller daughter vesicles from a parent GUV as a result of spontaneous tubulation shown in Figure S2. Ternary mixtures of DOPC:DPPC:Chol were also employed in order to understand the role of membrane heterogeneity and membrane stiffness. Large scale membrane fluctuations/deformations has been captured as a result of QD binding as presented in Figure S3. In order to locate the position of the QD, the experiment has also been performed on untagged GUVs. Confocal images obtained from the QD signals indicates binding of particles to the rim of the DLPC GUV and were not encapsulated inside the GUV compartment as shown in Figure S4.

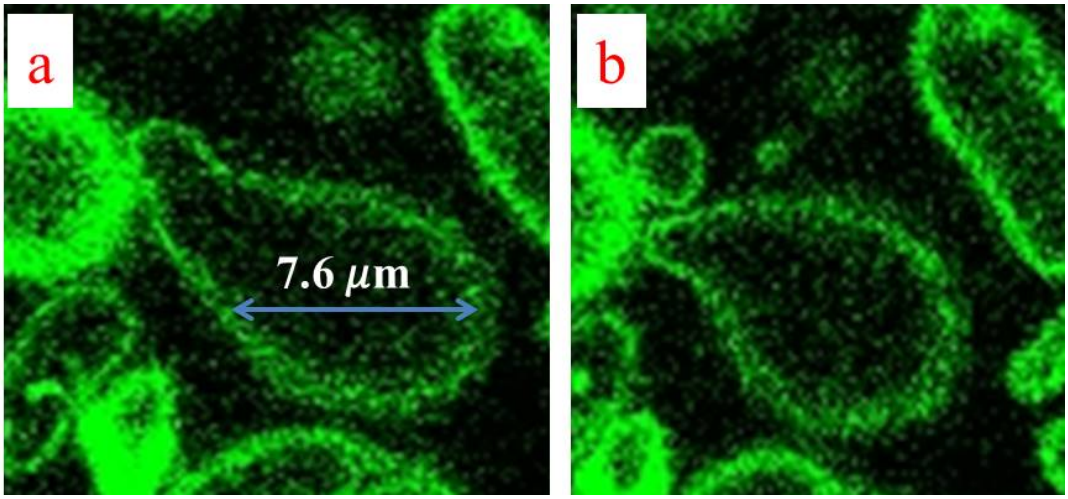

Fig. S2. Confocal images of DLPC GUV that results in vesicles budding from a parent GUV on binding of QD (a) Bud developed from the GUV (b) Daughter vesicle bud off from the mother vesicle

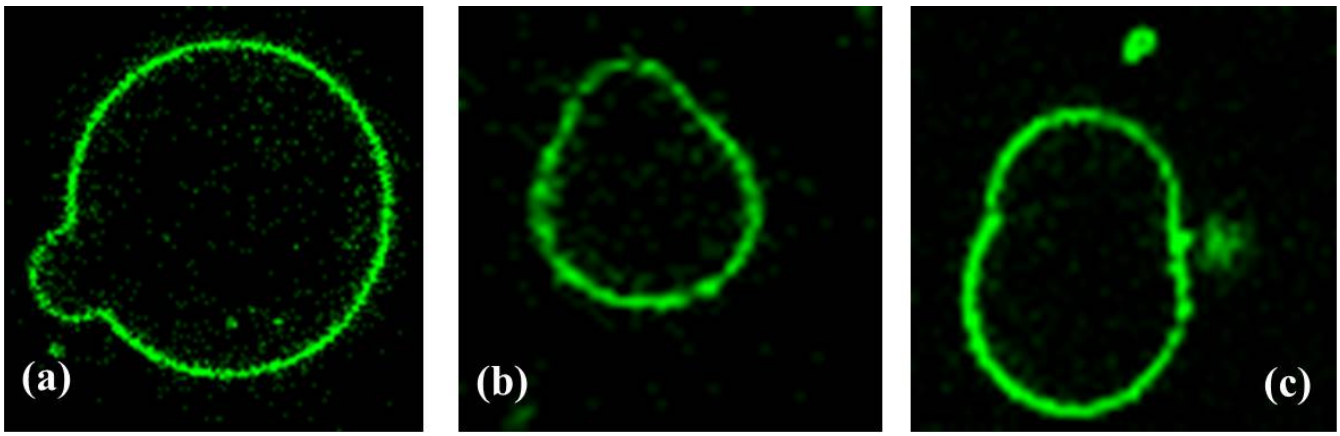

Fig. S3. Confocal images of three componenent GUVs exhibiting membrane deformations on QD binding

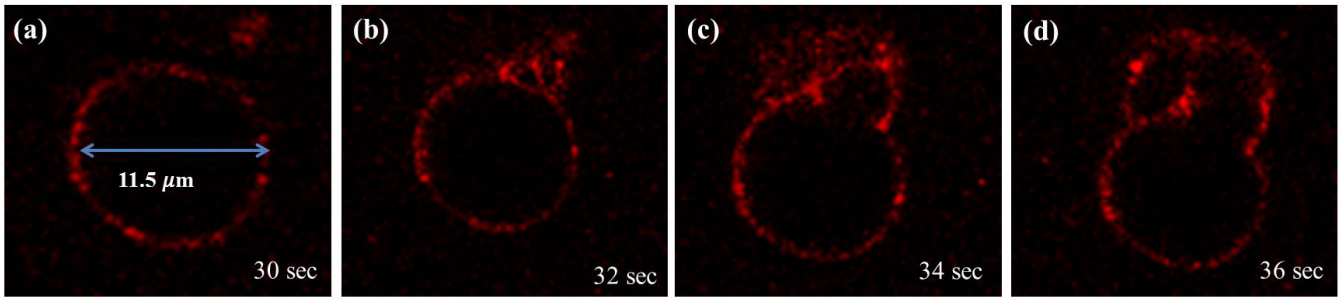

Fig. S4. Confocal images of an untagged DLPC GUV after incubation of QD.

E. (v) Time evolution of Lipid tubules. The crux of this work is on quantification of Tubelength (L_T) with time and characterizing the mechanical properties of the tubes corresponding to different L_T regimes. It has been presented in the main text that the evolution of tubules such as emergence, evolution and retraction are influenced by the membrane phase, membrane heterogeneity and QD concentration (Fig. F1 and F3). In order to capture the evolution of tubules and quantify the process, time series images for all the composition and QD concentration has been carried out as shown in Figures S5 - S9. Following observations could be made with respect to the confocal images. Tubule evolution involves initiation, growth, saturation and retraction as discussed in main text. Retraction of tubules is delayed in DMPC and L1P0 (low concentration). This observation suggests that stiffer membrane delays tube retraction as opposed to fluidic membrane that delays tube onset (Fig. F2 and Table T1). Homogeneous tubulation has been captured for single component system for all compositions and concentrations as opposed to phase specific tubulation events in case of two component system.

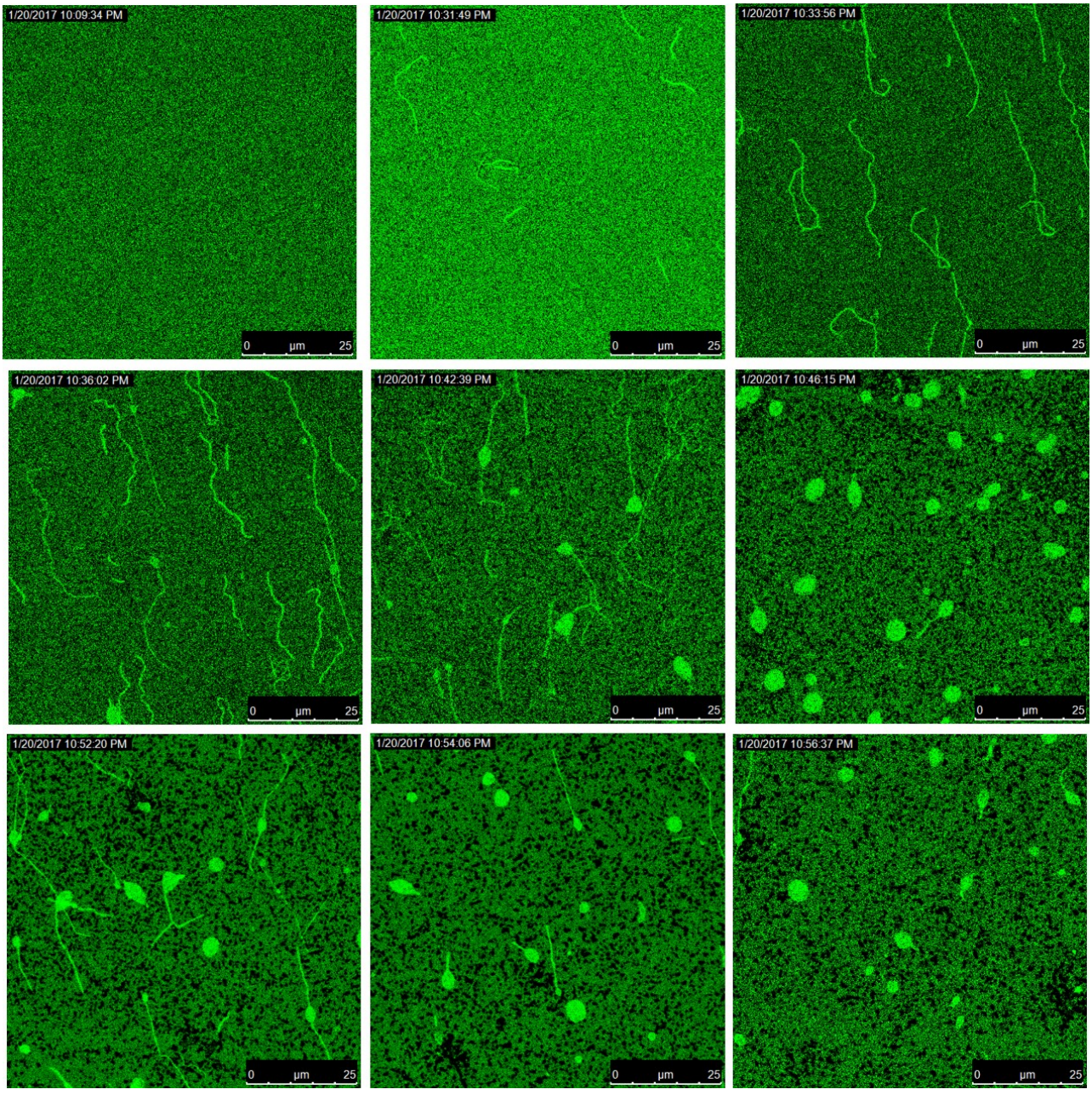

Fig. S5. Tubules Evolution in DLPC

F. (vi) Lipid Intensity on the Tubules. All quantification carried out in this study are primarily based on the time dependent confocal measurements. As a result, time dependent fluorescence signal from the system of interest has also been effectively captured. Hence, fluorescence intensity from the lipids and QDs present both in the membrane as well as in the tubes could be captured with time. With respect to membrane lipid signal (Fig. S10), counts reduce with reference to the time of onset of tubules due to supply of lipids from the membrane to sustain tube growth. Interesting trends of QD counts on tube has been discussed in the main text in the context of QD binding-unbinding and subsequent effect on tubulation kinetics.

G. (vii) Nature of Lipid Tubules. Confocal images has been extensively used in this study to understand the nature of kinetics and evolution of lipid tubules an its properties. Large area images presented in the main text projects the lipid tubules as bright thread like features. However, the nature of these tubules are hollow structures as shown in Fig. S11. This image has been obtained with a line average of 8 and frame average of 4 for a better S/N ratio and clean image. It was also post-processed using LEICA software.

H. (viii) QD concentration. Effect of membrane heterogeneity has been discussed in the earlier sections. Similarly, QDC concentration also plays a crucial role in determining the nature of membrane deformation. In an earlier reported work (3), fluidic DLPC bilayer were chosen to study the effect of QD concentration in tuning the membrane structural re-organization. Membrane structural perturbation was noticeably captured only above a threshold QD concentration of 1 nM. Threshold concentration requirement is an indication of effect of co-operative effect of QD. Figure S12 shows the different membrane re-organization for 3 different concentrations. Membrane turns porous with lipids re-organizing for 1 nM as shown in Fig S12 Panel A. With further rise in concentration (4 nM), tubulation occurs. For higher concentrations, lipid-enriched domains are captured. These features are quite similar in structure to the tubule retracted state. Hence, it is possible that for concentrations above 4 nM, tubulation onset and retraction happens too quickly to be captured with the temporal sensitivity of our measurements. As discussed in the main text, concentration plays a very crucial role in determining the kinetics of the tubule evolution.

I. (ix) Membrane Heterogeneity. In case of two component membranes, DLPC:DPPC has been designated as LxPy where x and y denotes the respective composition/fraction. QDs bind homogeneously onto the membrane resulting in homogeneous membrane deformations distributed uniformly throughout the bilayer unlike the two component bilayers. Interestingly, QD binding has been observed to be preferentially towards F-Phase compared to S-Phase of L1P1 as shown in Fig S13. These results suggests that single component bilayer facilitates non-specific binding whereas two component bilayers with presence of membrane heterogeneity drives specific binding towards fluid domains. In addition, QD binding has been observed to be enhanced in L1P1 compared to the simple homogeneous DLPC bilayer (4).

Figure S14 shows L1P1 bilayers that exhibits bright dye enriched S-phase (DPPC rich) and dye devoid F-phase (DLPC rich). Subsequent to addition of QD, membrane turns homogeneous and further fluorescence intensity of F phase increases with a drop in the intensity of S phase as a result of the nature of binding of the QD (Fig S14). Further, lipid tubules were observed to emerge specifically from the F phase only as discussed in main text and shown in Figure 2 and Figure S15. Hence, lipid re-organization between the two phases suggests of co-operative behaviour between F and S phase that finally results in emergence of tubulation specifically from one phase.

J. (x) Compressibility of L1P1 membranes. Supported lipid bilayers (SLBs) has been prepared using Langmuir Blodgett Technique at specific surface pressure. Surface pressure gets monitored using Wilhelmy plate. Target pressure (lipid packing) can be controlled through compression of the Teflon barriers. During each transfer of a LB film, respective pressure-area isotherms gets captured. Further analysis on the isotherms can be performed to extract the compressibility modulus (δ). Compression isotherms for different mixtures of DLPC and DPPC is shown in Figure S16. Comparison of δ for different mixtures of DLPC and DPPC is presented in Figure S17. It follows that the values of L1P0 and L1P1 is quite similar in its stiffness as quantified in terms of δ. The membrane stiffness has been observed to increase only for DPPC fraction more than 50%. Absence of tubule formation in L0P1 seems to have strong correlation with its stiffness as observed in Figure S17.

L1P1 bilayer exhibits unusually early onset of both tubulation and retraction as shown in Fig. F2 and Table T1. In order to understand this, results of different complementary studies have been correlated. Interesting anomaly of δ properties of L1P1 has been shown in Figure S17. Similarly, lipid dynamics study in L1P1 using Fluorescence Correlation Spectroscopy (FCS) suggests that fluidity of DLPC rich F-phase is slightly faster than the DLPC diffusivity (pristine reference) as shown in Figure S18. This trend of enhanced diffusivity in F-phase has been observed till 50% of DPPC in the SLB composition. Subsequent to this DPPC lipid concentration, slow diffusion has been captured in F-phase. However, as expected lipid diffusion in DPPC rich S-phase has always been observed to be lower than the DLPC bilayer. Hence, in diffusivity studies as well, L1P1 shows non-monotonic trends. For any slight increase in concentrations above this, membrane shows stiffness in its properties and response.

K. (xi) Estimation of L_T and L_P. Figure S19 shows the method of estimation of L_T from a confocal image captured at a given time.

Persistent Length (L_P) analysis was executed using Easyworm, open-source tool to estimate the mechanical parameters of polymers and provides information about the flexibility of tubes specific to each sample. L_P of semi-flexible polymers were calculated using worm-like chain model. Tubules/Polymers are fitted to parametric splines by Easyworm. It is an user-friendly

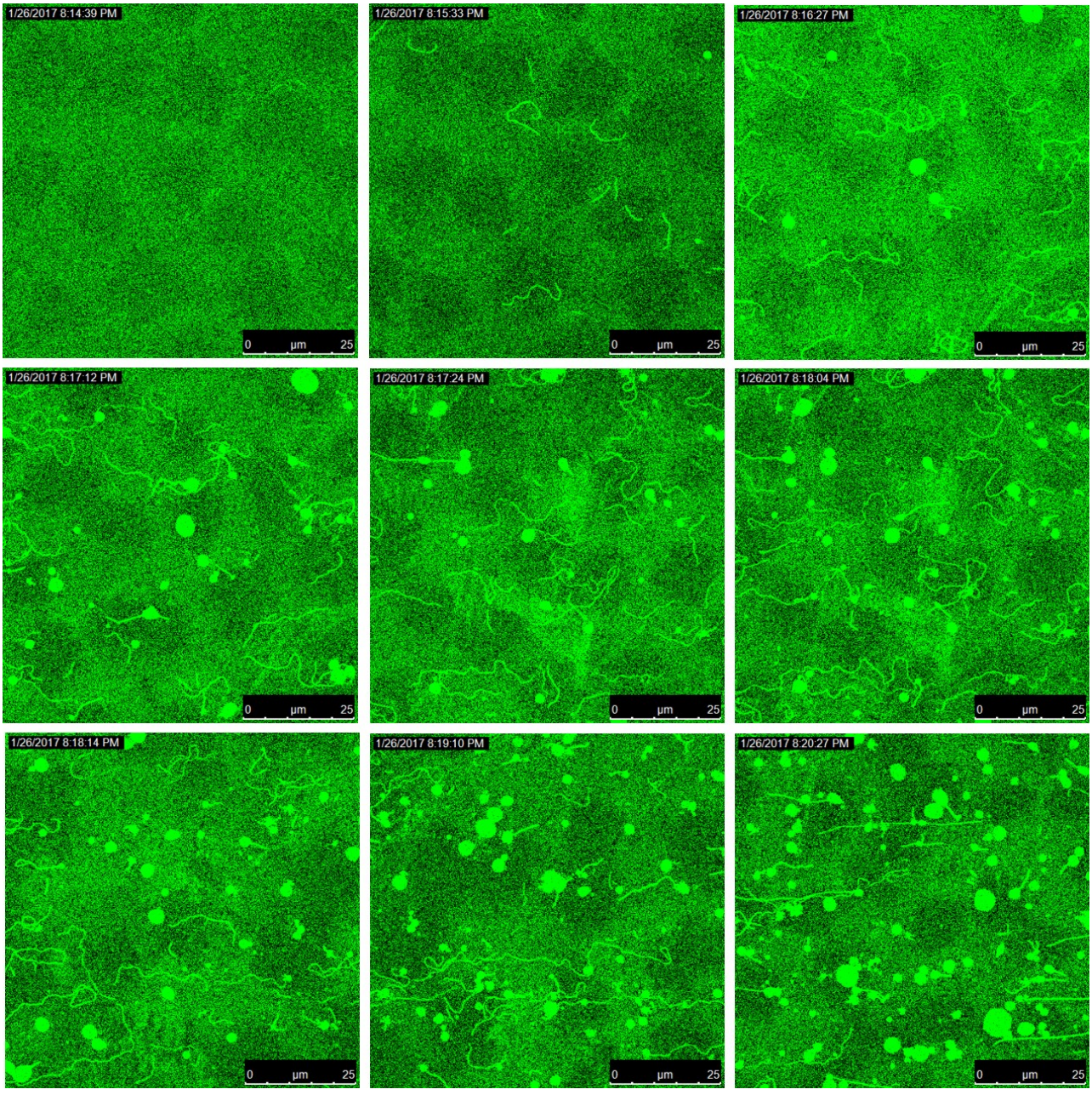

Fig. S6. Tubules Evolution in L1P1

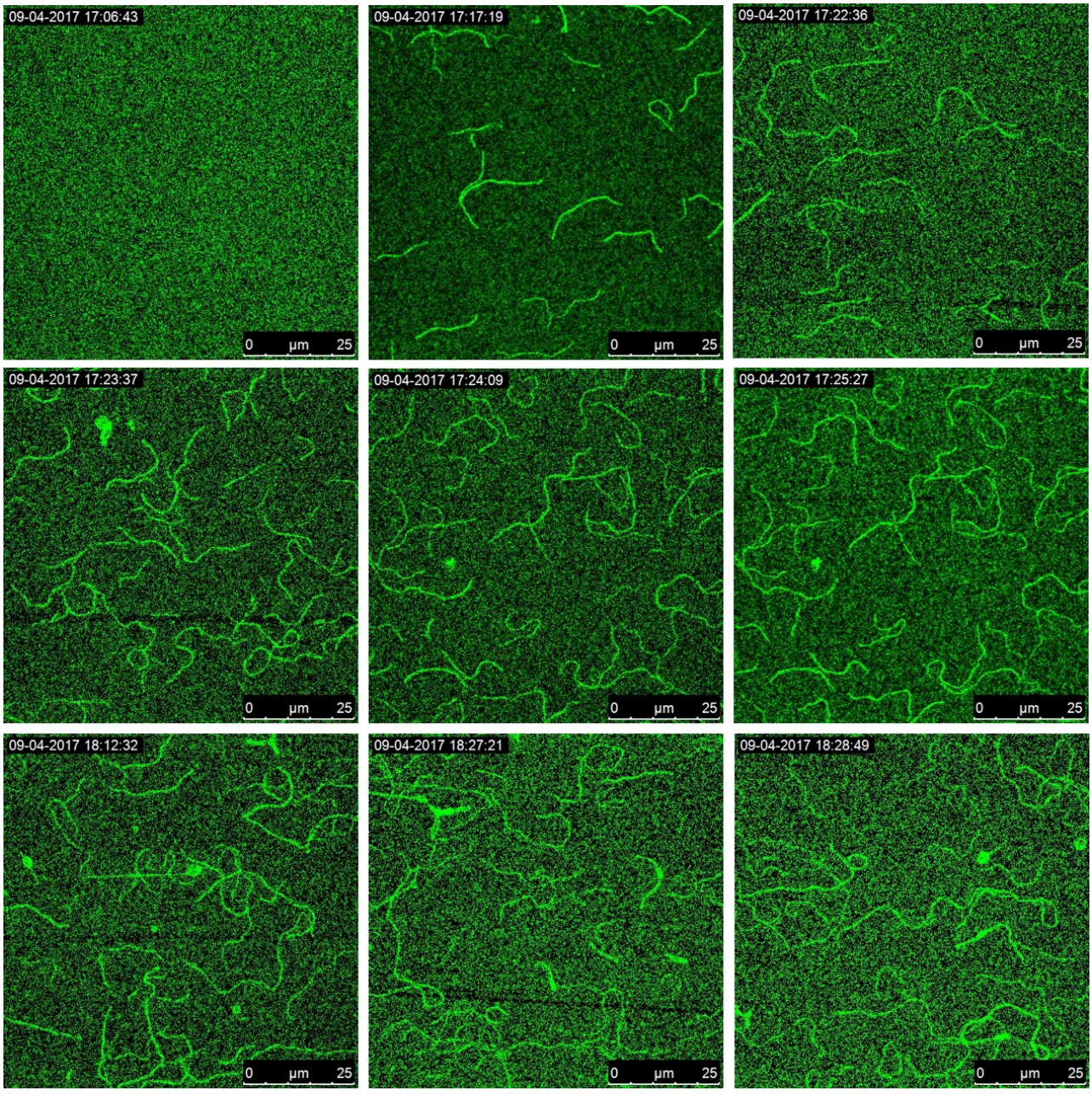

Fig. S7. Tubules Evolution in DMPC

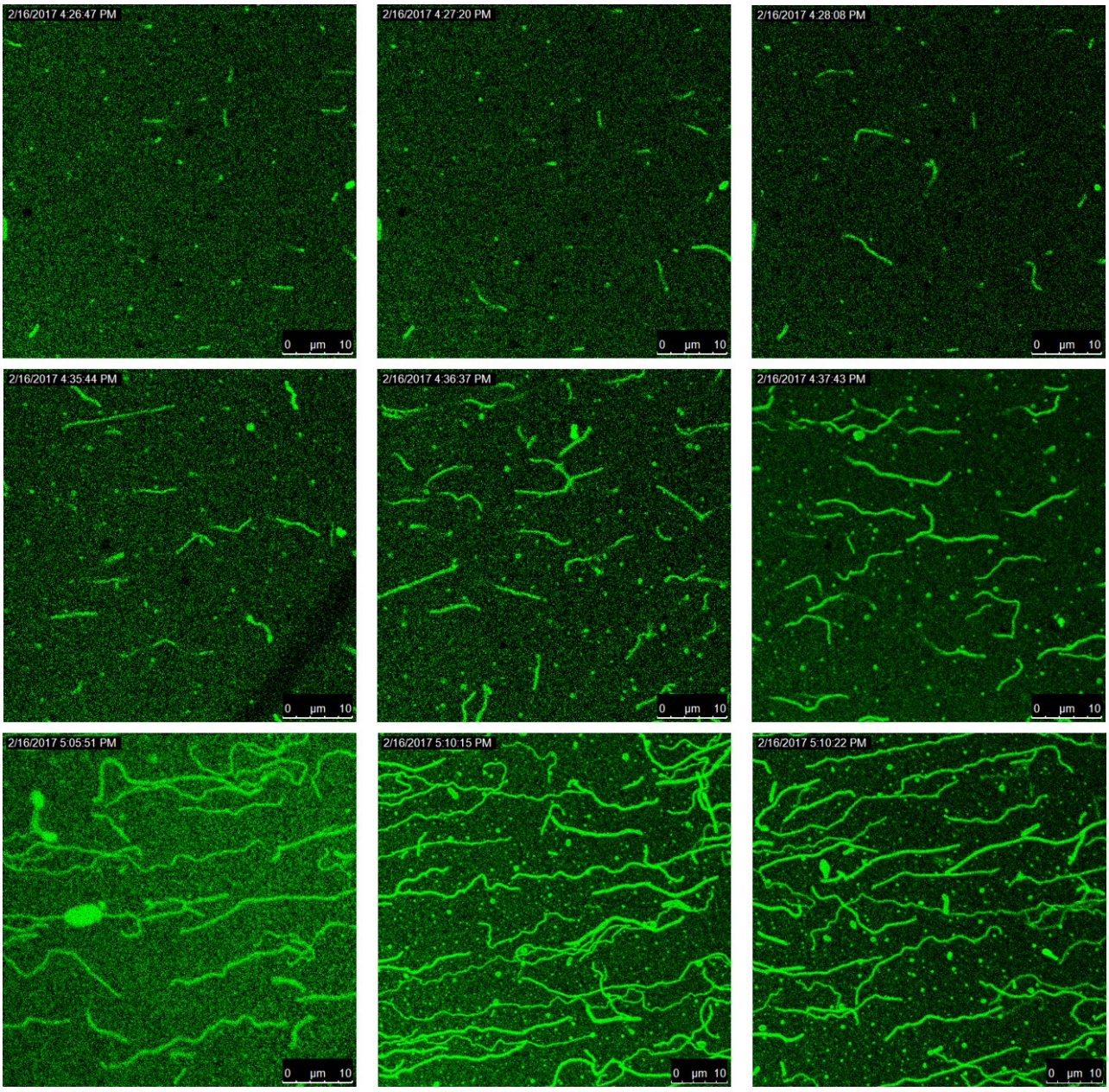

Fig. S8. Tubules Evolution in DLPC for low QD concentration

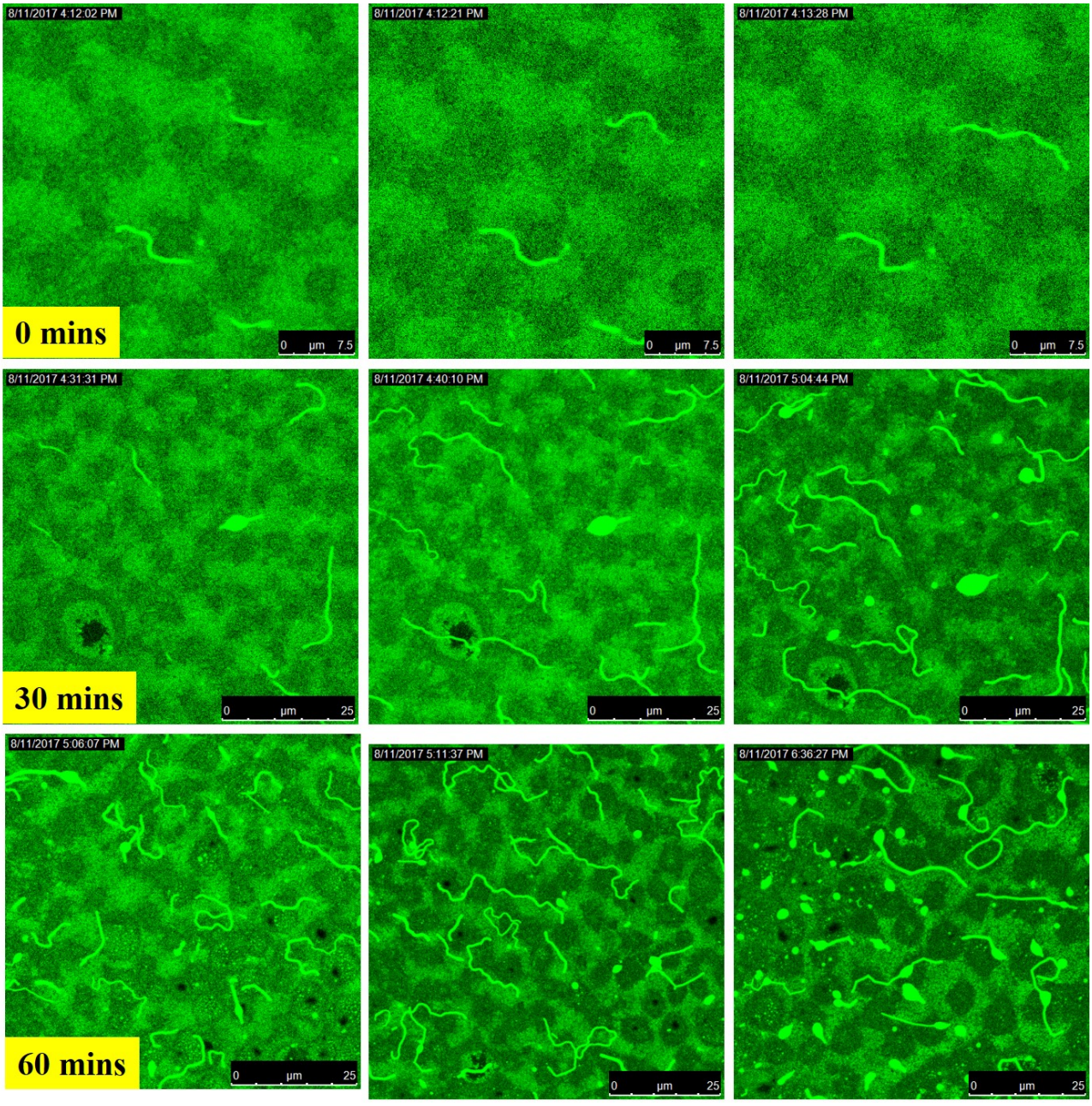

Fig. S9. Tubules Evolution in L1P1 for low QD concentration

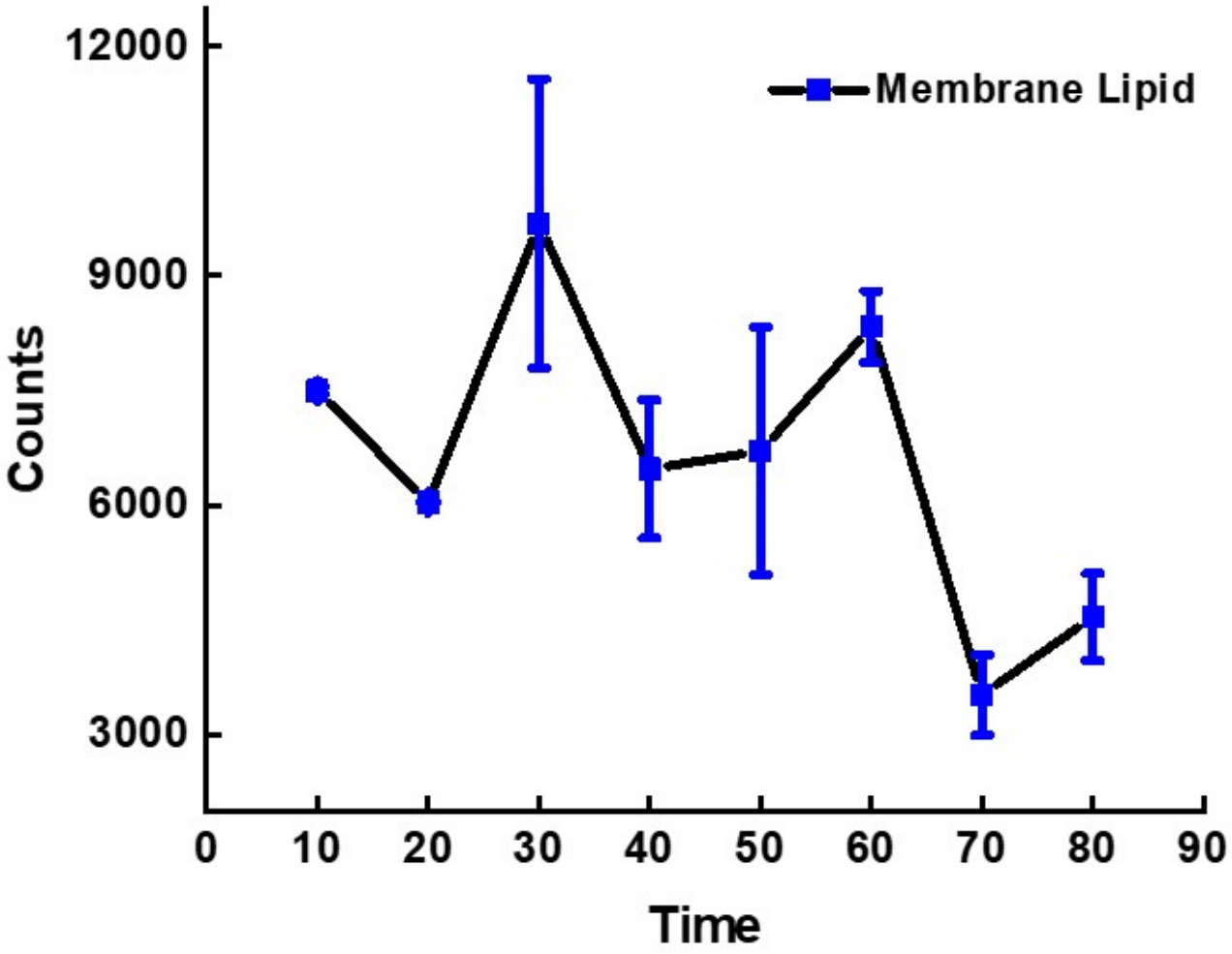

Fig. S10. Time dependent Intensity counts quantified on the membrane indicating drop in the membrane during the course of tubule generation and evolution. Counts has been quantified by choosing a square ROI on the membrane.

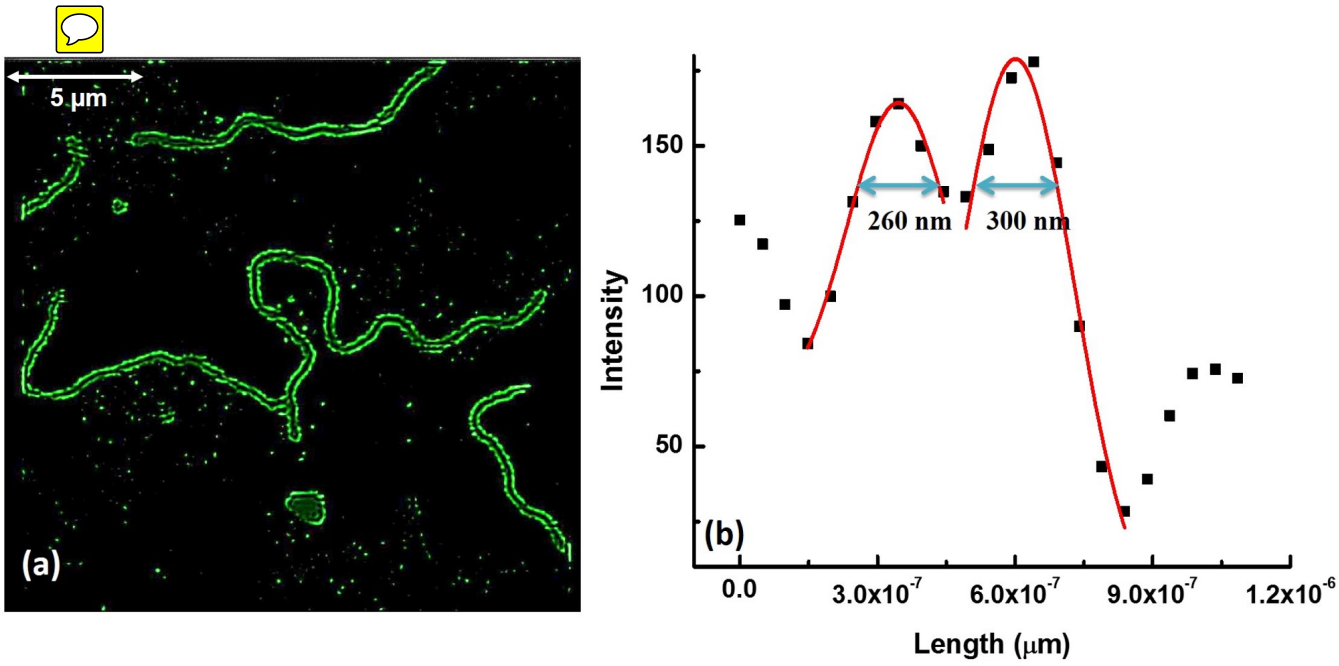

Fig. S11. Hollow nature of the lipid tubules captured using confocal imaging and subjected to de-convolution processing

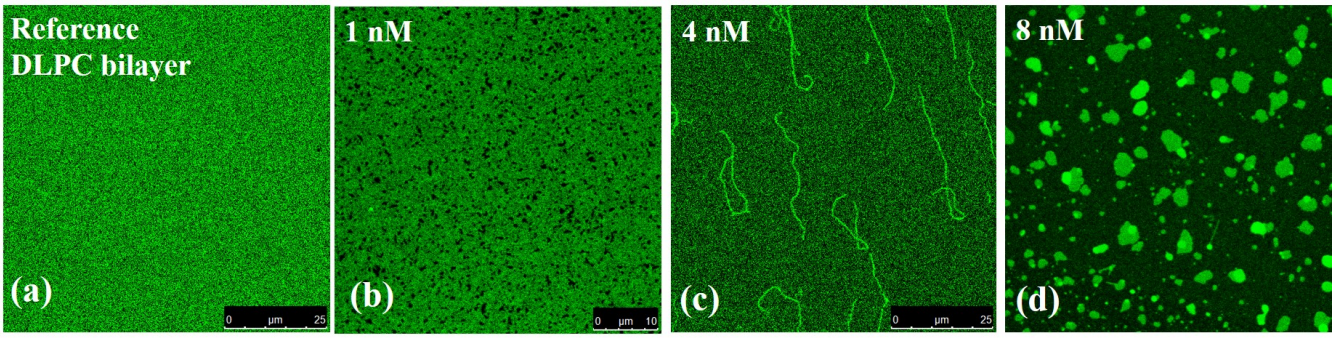

Fig. S12. (a) DLPC reference bilayer, Effect on membrane structure for QD concentrations corresponding to (b) 1 nM, (c) 4 nM and (d) 10 nM.

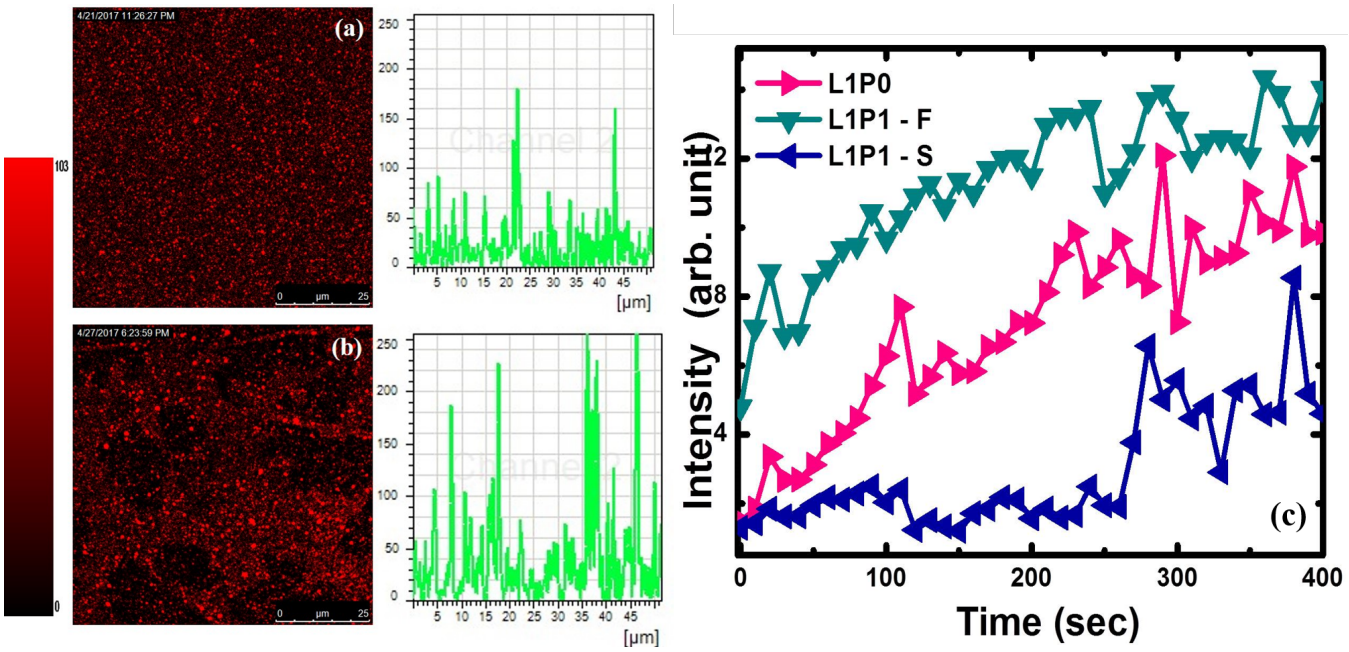

Fig. S13. QD signal on (a) DLPC and (b) L1P1 (c) Comparison of time dependent fluorescence intensity.

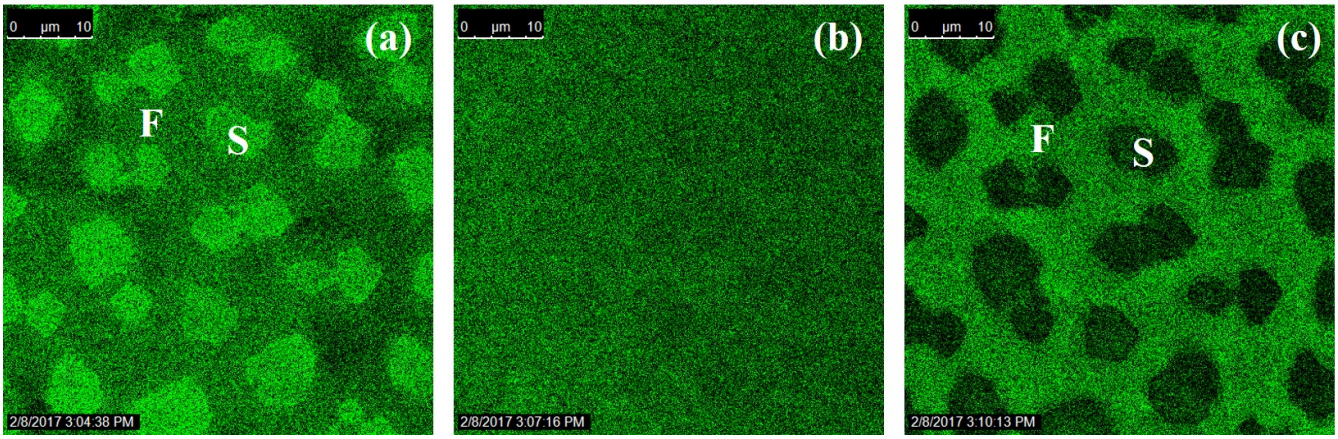

Fig. S14. Confocal imaging of (a) L1P1 pristine with bright S phase and comparatively dark F phase (b) Immediate to addition of QD, SLB turns homogeneous briefly and (c) Membrane re-organizes with S phase turning dark and F-phase turning bright

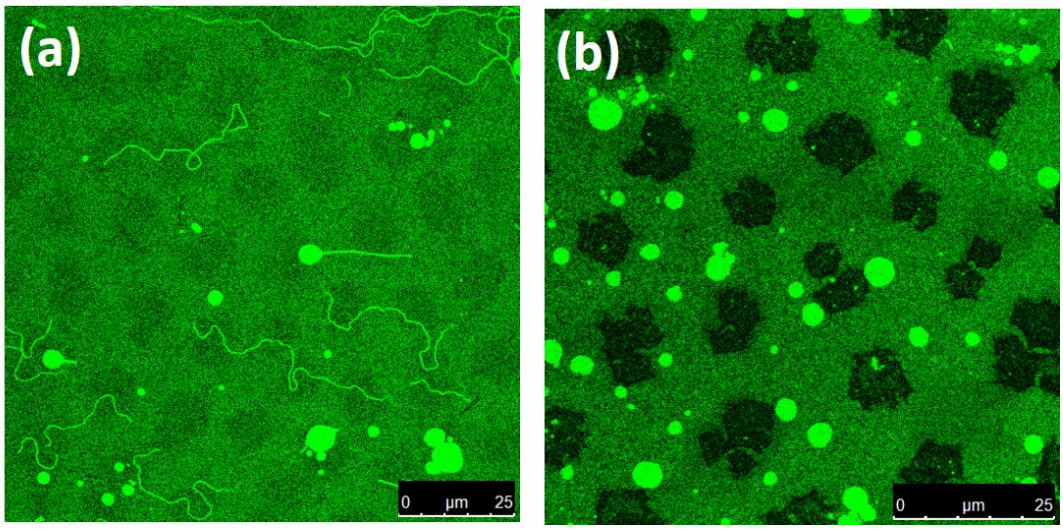

Fig. S15. Features evolving only from the F-phase of the SLB (a) Tubules at concentration of 4nM (b) Circular domains for concentration of 10 nM

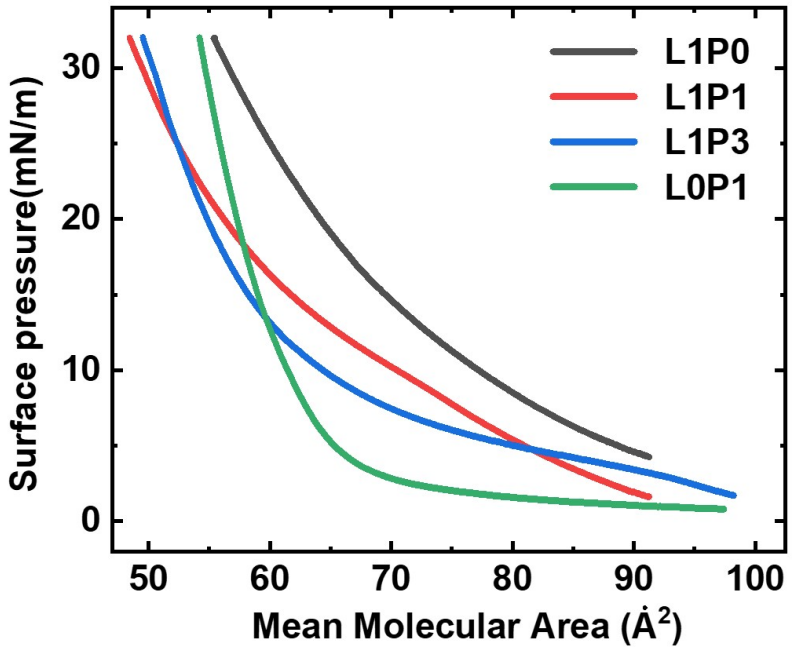

Fig. S16. Langmuir Isotherms
Comparison of isotherms for different mixtures of DLPC and DPPC

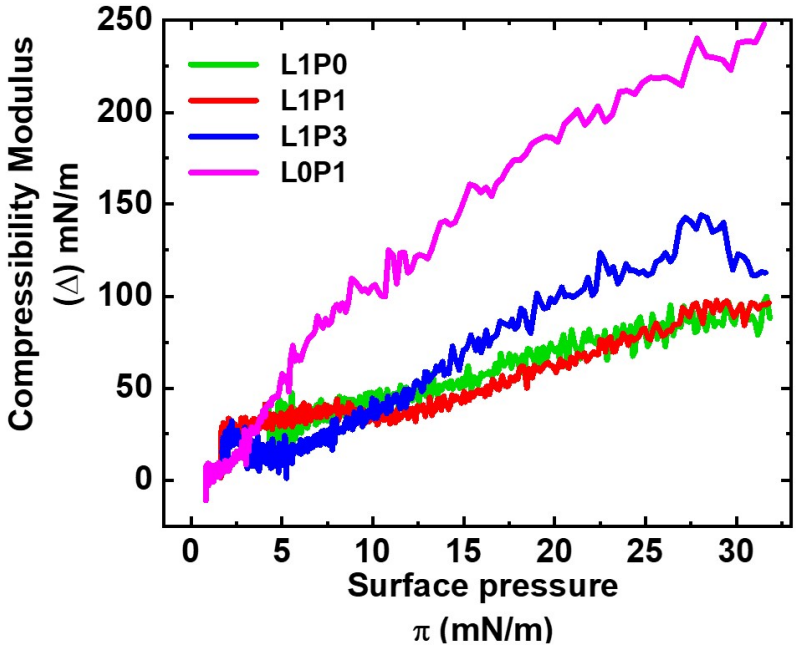

Fig. S17. Compressibility Modulus $\delta/$

Compressibility modulus of the lipid monolayer extracted from Langmuir monolayer Isotherms. Raw data obtained in Langmuir-Blodgett experiment has been used in calculation of κ.

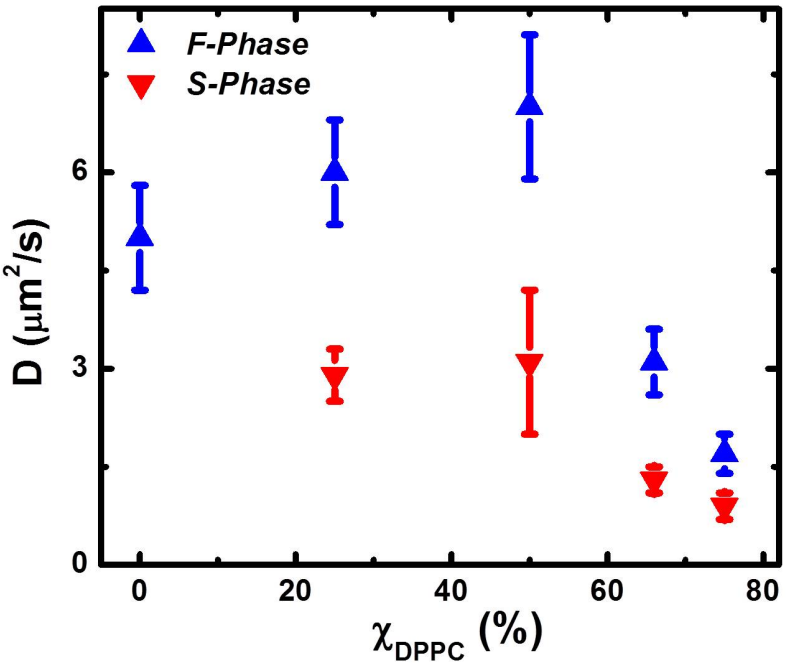

Fig. S18. FCS based lipid diffusion measured in F-phase (Blue code) and S-phase (Red code) for different compositions of DLPC and DPPC.

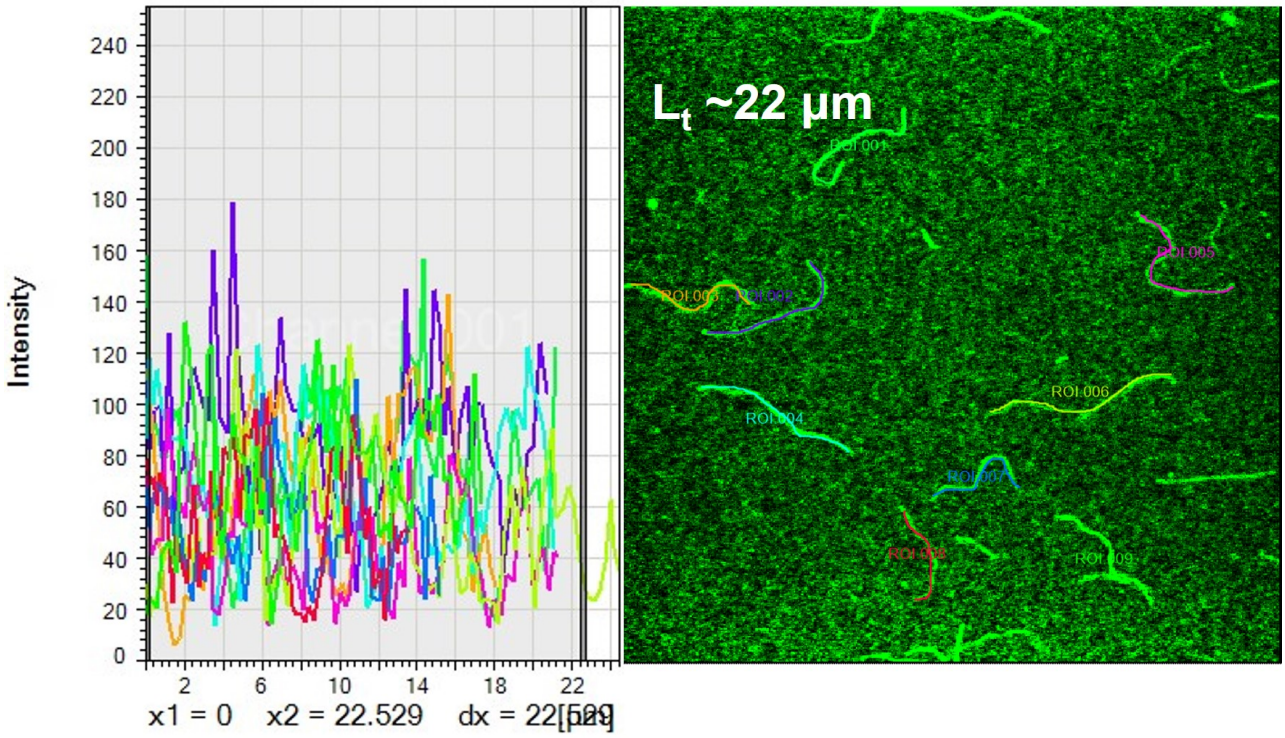

Fig. S19. Methodology of Quantification of L_T from the confocal images

and ready to use, Graphical User Interface in MATLAB. It is optimized for analyzing polymer chains captured using Atomic Force Micrscopy, Optical Microscopy, Electron Microscopy with minimal user inputs. These analyses have been performed using Easyworm software (GUI, MATLAB) (5). Easyworm has been coded with two different methods to calculate L_P : (i) tangent-tangent correlation, (ii) mean square end-to-end distance as a function of length shown in Figure S20. Eqn. SE1, SE2 have been defined earlier in the main text.

$$< R^2 >= 2sL_Pl\ (1 - \frac{sL_P}{l}(1 - e^{-\frac{l}{sL_P}})). \quad [1]$$

where κ - bending rigidity, K_B - Boltzmann constant, T the experimental temperature, r - radius of the lipid tubules, $< R^2 >$ - mean squared of the end-to-end distance as a function of length l, S - surface parameter which has been set to a value of 2 for chains equilibrated on 2D surface. S parameter reflects the influence of surface free energy of the substrate and lies between 1 to 2. For fully equilibrated chains, in case of 2D, this values is chosen as s=2; in 3D it is chosen as s=1. For fluctuations between 2D and 3D, it is approximated as s=1.5

$$< cos\theta >= \exp^{\frac{l}{sL_P}} \quad [2]$$

θ - angle between two segments of the tube separated by a distance l along the tube contour.

Execution of this analysis using Easyworm is simple and user friendly. Confocal image for a given time frame will be exported as .tiff format. Details such as image size and resolution has to be given as inputs to the GUI. Each chain has been manually selected by drawing a line profile across the entire length of the tubules capturing all visible flexibility of the tubes. On providing these data, a second GUI gets loaded with details of number of tubes, number of contours (segments) to be chosen in the tube, iterations in the fitting. On launch of fit, Persistent length values are extracted using both end-end correlation and tanget correlation.

L_P analysis for high QD concentration has been presented in main text. Similar analysis has been executed for lower QD concentration as shown in Figure S21. Interestingly, the non-monotonic trends in L_P analysis is reflected in low QD concentration study as well. However, stiffness of the lower QD tubes seems to be slightly on the higher side compared to its counterparts.

References

1. JC Stachowiak, CC Hayden, DY Sasaki, Steric confinement of proteins on lipid membranes can drive curvature and tubulation. *Proc. Natl. Acad. Sci.* **107**, 7781–7786 (2010).
2. Y Yu, S Granick, Pearling of lipid vesicles induced by nanoparticles. *J. Am. Chem. Soc.* **131**, 14158–14159 (2009).
3. R Chelladurai, JK Basu, Charged nanoparticle induced pattern formation and dynamic re-organisation on model biomembranes. *J. Phys. D: Appl. Phys* **51**, 304002 (2018).
4. R Chelladurai, K Debnath, NR Jana, JK Basu, Nanoscale heterogeneities drive enhanced binding and anomalous diffusion of nanoparticles in model biomembranes. *Langmuir* **34**, 1691–1699 (2018).
5. G Lamour, JB Kirkegaard, H Li, TP Knowles, J Gsponer, Easyworm: an open-source software tool to determine the mechanical properties of worm-like chains. *Source Code Biol. Med.* **9**, 1–6 (2014).

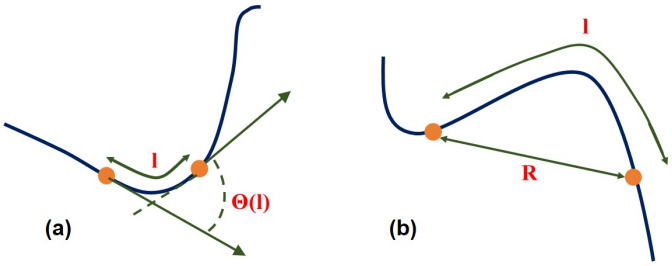

Fig. S20. Methods to calculate L_P (a) theta-theta correlation (b) mean square of the end-to-end distance correlation

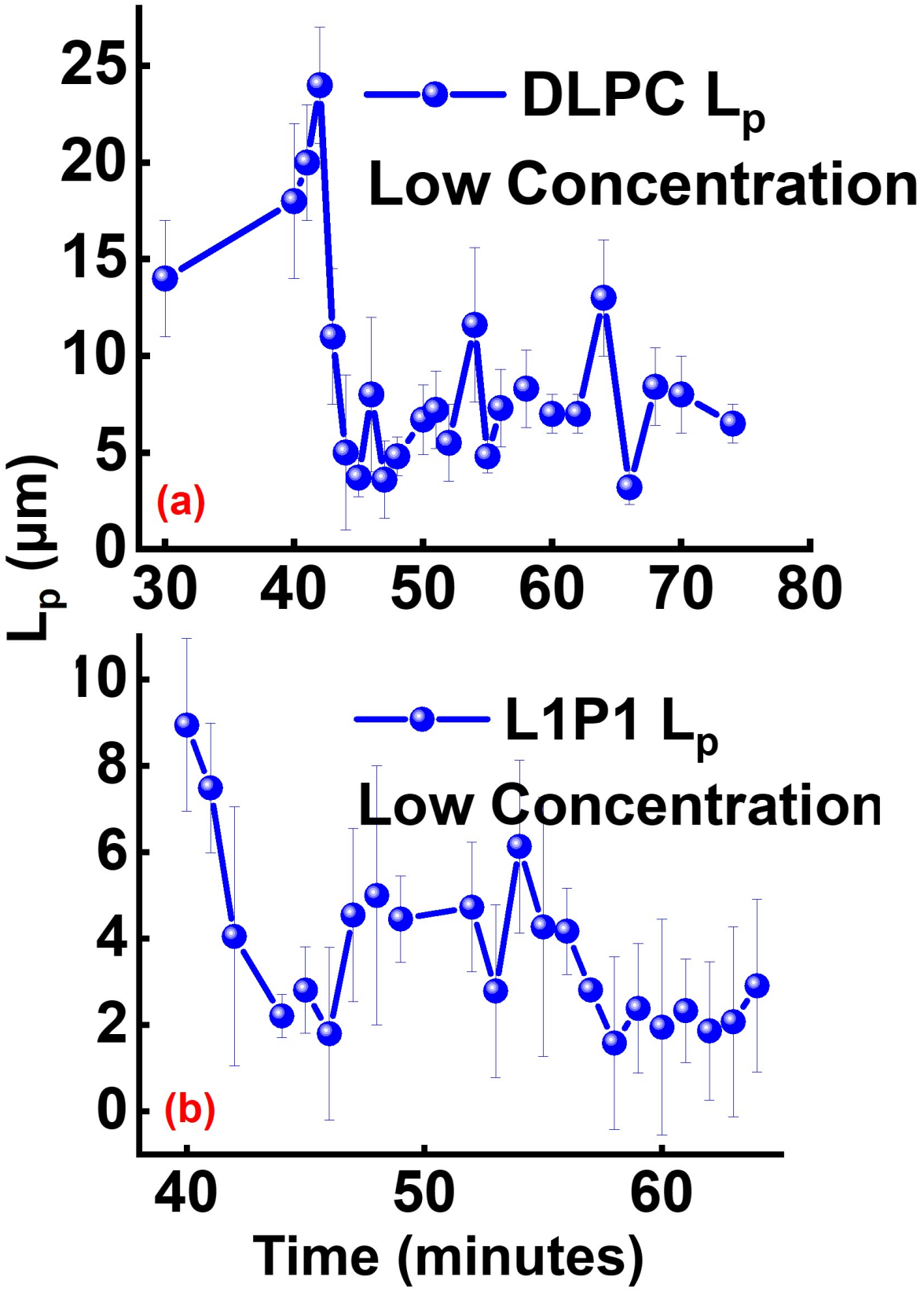

Fig. S21. Persistent Length Analysis for low QD concentration 2nM(a) DLPC bilayer (b) L1